Eurographics/ ACM SIGGRAPH Symposium on Computer Animation (2006)
M.-P. Cani, J. O'Brien (Editors)

# A Consistent Bending Model for Cloth Simulation with Corotational Subdivision Finite Elements

Bernhard Thomaszewski[1] Markus Wacker[1,2] Wolfgang Straßer[1]

[1]WSI/GRIS, Universität Tübingen, Germany
[2] Institut für Mathematik/Informatik Computer-Graphik, HTW Dresden, Germany

**Abstract**

*Wrinkles and folds play an important role in the appearance of real textiles. The way in which they form depends mainly on the bending properties of the specific material type. Existing approaches fail to reliably reproduce characteristic behaviour like folding and buckling for different material types or resolutions. It is therefore crucial for the realistic simulation of cloth to model bending energy in a physically accurate and consistent way. In this paper we present a new method based on a corotational formulation of subdivision finite elements. Due to the non-local nature of the employed subdivision basis functions a $C^1$-continuous displacement field can be defined. In this way, it is possible to use the governing equations of thin shell analysis leading to physically accurate bending behaviour. Using a corotated strain tensor allows the large displacement analysis of cloth while retaining a linear system of equations. Hence, known convergence properties and computational efficiency are preserved while convincing and detailed folding behaviour is obtained in the simualtion.*

Categories and Subject Descriptors (according to ACM CCS):
I.3.5 [Computer Graphics]: Physically based modelling

**Keywords:** Cloth simulation, polar decomposition, thin shells, subdivision surfaces, finite elements

## 1. Introduction

Physically-based modelling has become the de facto standard in cloth simulation. For dynamically deformable surfaces, mass-spring systems continue to be the most widely used simulation technique in computer graphics due to the low computational cost and easy implementation. While this method already provides some parameters with physical interpretation, homogeneous materials cannot be simulated consistently. For authentic material mapping and hence realistic and reliable draping behaviour of cloth, as required e.g. by the textile community, one must necessarily resort to continuum mechanics. In doing so, material behaviour can be reproduced accurately and independent of discretisation throughout a broad range of resolutions. Generally speaking, each continuum formulation results in a set of partial differential equations (PDEs) which has to be discretised in space and time. The spatial discretisation is usually carried out by means of finite differences (FDM) or finite element methods (FEM). While a remarkable amount of effort has been spent on precisely reproducing the in-plane forces, few ex-

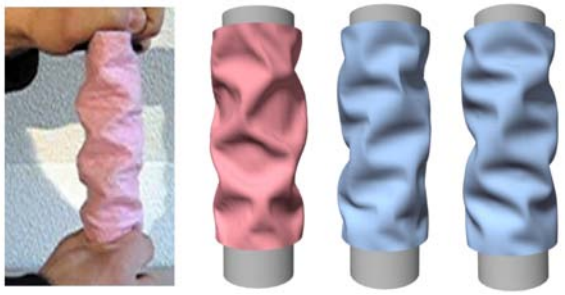

**Figure 1:** *Typical folding patterns on real and simulated fabric using different methods.* Left*: Buckling due to compressive deformation on a real fabric sample.* Middle*: same compression state simulated with our method (red). The folds and specifically the size of the diamond-shaped buckling pattern are reproduced accurately.* Right*: a standard approach using simple bending with the same mesh (2232 vertices) does not yield convincing results (blue). Moreover, using a finer mesh (5856 vertices) the result does not get qualitatively better although it visually changes substantially.*

isting models are concerned with an accurate and consistent way of modelling bending energy. Nevertheless, the characteristic folding and buckling behaviour of cloth (see Fig. 1) highly depends on bending properties. From the field of engineering, the thin plate equations are known to be an adequate approach to this problem. However, they have not yet been successfully applied to dynamic cloth simulation. This is due to the fact that the associated minimisation problem includes 4th order derivatives with respect to the displacements. A corresponding finite element approach therefore requires a $C^1$-continuous displacement field (to be exact the shape functions have to be in $H^2$). The main problem with this requirement is guaranteeing continuity across elements which usually necessitates the use of additional variables (e.g. slopes). Recently, Cirak et al. [COS00] elegantly solved this problem through the introduction of subdivision basis functions to finite element analysis. This approach was originally intendend for static analysis only and we therefore extend it to fully dynamic textile simulations. This also implies that the frames are not only calculated as a sequence of quasistatic rest shapes. Instead, we solve the full time dependent differential equations (cf. eq. (28)). In order to keep the convergence properties of a linear approach and at the same time account for arbitrarily large rigid body transformations we use a corotated strain measure. Unlike in former approaches the physically accurate treatment of bending leads to an energy minimisation including both membrane and bending contributions. This, coupled with an implicit time integration scheme stability ensures that stability issues never arise.

## 2. Related Work

Throughout the last two decades there has been a lot of interest in cloth simulation and animation. A complete discussion of the relevant work is beyond the scope of this paper and the reader is therefore referred to the textbook by House and Breen [HB00], Volino and Thalmann [VMT00] or the overview compiled by Ng and Grimsdale [NG96] and Volino et al. [VCMT05]. In the following, we classify the previous work relevant to the presented approach into different categories.

**FEM** Finite element methods have not yet seen much attention in cloth simulation – at least not in computer graphics. While we only mention the most relevant work here an extensive list can be found in [HB00]. Most of the existing FE-approaches are based on the geometrically exact thin shell formulation presented by Simo et al. [SF89]. Eischen et al. [EDC96] depart from the fully nonlinear theory and apply it to cloth simulation using quadrilateral, curvilinear elements. Because of the buckling behaviour of cloth which can lead to divergence in the algorithm an adaptive arc-length control is used. Etzmuss et al. [EKS03] presented a linear FE-approach based on a plane-stress assumption. Bending is treated separately from in-plane deformation while a corotational strain formulation is used to account for arbitrary rigid body transformations. Cirak et al. [COS00] use the formulation of [SF89] to derive equilibrium equations. They introduce a new kind of element based on subdivision basis functions. Unlike former FE-formulations $C^1$-continuity is ensured by the nonlocal nature of the element shape functions while retaining linearity in the displacements. The method was later extended to the finite deformation range using nonlinear theory [CO01, GCSO99].

**Corotational Formulation** The extraction of the rotational part from the displacement field used in [EKS03] was first addressed by Müller et al [MDM+02] who used a warping heuristics. However, due to the inaccuracy of this method occuring *ghost forces* have to be treated separately. A more precise method was presented by Hauth et al. [HS04] who used the polar decomposition of the deformation gradient. While the latter work proposes an iterative solution for the 3D case, Etzmuss et al. [EKS03] take a direct way for the simpler 2D problem. In our approach, the rotation field is extracted in a similar way. This allows stable treatment of arbitrarily large rigid body transformations and strict separation of curvature and membrane strains.

**Bending Models** Most of the existing cloth simulation techniques use an angular expression to model bending energy or forces. Breen et al. [BHW94] use the linear beam theory relating bending moment to curvature. Curvature is approximated by fitting a circle to the three points defined by two incident edges. A biphasic expression in terms of the enclosed angle is then used for approximation. Volino et al. [VCMT95] use a similar approach but rely on the dihedral angle formed by two neighbouring triangles. Choi and Ko [CK02] propose a bending model simultaneously accounting for compression and buckling. Specific assumptions on the post-buckling state and associated energy lead to the derivation of bending forces. Bridson et al [BMF03] identify an independent bending mode where the requirement is to not affect rigid body motions and in-plane deformations. Thus, they derive directions and relative magnitudes for the bending forces of a basic bending element consisting of two neighbouring triangles. Grinspun et al. [GH+03] use a discrete mean curvature approximation for a sound definition of bending energy for flexible shell-like objects. Because the necessary gradient computation is intricate the use of automatic differentiation is suggested. A method to use thin shell dynamics with point sampled surfaces for efficient animation was recently proposed by Wicke et al. [WSG05]. This approach is particularly useful for scenes where the topology changes due to cutting or tearing. However, the method is limited to explicit time integration and the accuracy of the computational framework (e.g. boundedness of the solution) is not clear.

In most of the above mentioned approaches, the treatment of bending is physically motivated but not accurate. This

means that realistic material mapping and resolution independence cannot be expected. Since implicit time integration is mandatory for stable and efficient cloth simulation (see [BW98]) the approach by Wicke et al. is not an option. The methods by Bridson et al. and Grinspun et al. (which have in fact some aspects in common) are more promising. An implicit treatment of bending, however remains difficult as second order derivatives of the bending energy are then required. For this reason Bridson et al. use explicit integration for their directly derived bending forces. This works well with small enough time steps and materials without too strong a resistance to bending deformation. However, this method is not unconditionally stable anymore. On the contrary, Grinspun et al. treat bending implicitly and compute the required derivatives using automatic differentiation. Their method works well for inextensible rigid shells where the bending energy is largely predominant. For physically accurate cloth simulation, however, significant in-plane deformations can also occur and the interplay between bending and membrane energy needs to be treated consistently. Furthermore, their method is not founded on continuum mechanics. Therefore curvature and membrane strains are not explicitly available and modelling anisotropic materials becomes difficult. Additionally, independence of discretisation and convergence with higher resolution to the continuous equivalent at the same time is not given.

### 2.1. Overview and Contributions

We present an approach to cloth simulation which models both membrane and bending energy in a consistent and unified way. The physical basis for this method are the Kirchhoff-Love thin shell equations which essentially combine the theory of elastic membranes with the Kirchhoff thin plate analysis. The approach proposed by Cirak et al. [COS00] is extended to the fully dynamic case, and moreover we are able to account for arbitrary rigid body transformations. This is achieved through the use of a corotational strain formulation while preserving the linearity of the approach and thus retaining the associated advantages in convergence and computational efficiency. In addition, we present a simple method to incorporate various boundary conditions in the context of an implicit numerical solver. Finally, we compare the computational cost of our method to commonly used approaches.

## 3. Physical and Mathematical Modelling

In this section we will briefly describe the physical and mathematical background necessary for an understanding of our method. Throughout the remainder of this work Greek indices will take the values 1 and 2, Latin indices range from 1 to 3 and a comma denotes partial differentiation with respect to the subsequent variable. Additionally, the summation convention is assumed [Bar89].

### 3.1. Basics from Continuum Mechanics

A deformable solid in its current state is described by its configuration mapping

$$\varphi = \bar{\varphi} + u = id + u : \Omega \rightarrow \mathbf{R}^3 \,, \tag{1}$$

where $\Omega \subseteq \mathbf{R}^3$ is its parameter domain, $\bar{\varphi}$ the rest state and $u$ the displacement field. Here, we assumed that the rest state mapping is simply the identity. Let $\bar{\mathbf{v}}_1 \cdot \bar{\mathbf{v}}_2$ be the scalar product of two elemental vectors $\bar{\mathbf{v}}_i = \bar{\mathbf{p}}_i - \bar{\mathbf{q}}$ in the rest state with material points $\bar{\mathbf{p}}_i$ and $\bar{\mathbf{q}}$. Note that these vectors are related to their counterparts in the current configuration via

$$\mathbf{v}_i = \varphi(\bar{\mathbf{v}}_i) = \varphi(\bar{\mathbf{p}}_i) - \varphi(\bar{\mathbf{q}}) \,. \tag{2}$$

A general deformation measure can now be derived as the difference of scalar products in the rest and current state:

$$\mathbf{v}_1 \cdot \mathbf{v}_2 - \bar{\mathbf{v}}_1 \cdot \bar{\mathbf{v}}_2 = \bar{\mathbf{v}}_1 \cdot (\nabla\varphi^T \nabla\varphi - id) \cdot \bar{\mathbf{v}}_2 . \tag{3}$$

Using eq. (1) we can identify from eq. (3) the symmetric (nonlinear) Green strain tensor as

$$\varepsilon_G = \frac{1}{2}(\nabla\varphi^T \nabla\varphi - id) = \frac{1}{2}(\nabla u^T + \nabla u + \nabla u^T \nabla u) \,. \tag{4}$$

To investigate the internal forces related to a state of strain inside a deformable solid let $\Pi$ denote its total energy

$$\Pi = U + W \tag{5}$$

with elastic strain energy $U$ and potential energy $W$ due to applied forces. The strain energy is given in terms of the displacement field $u$ as

$$U = \int_\Omega \varepsilon(u) : \sigma(u) \, d\Omega \,, \tag{6}$$

where $\sigma$ is the symmetric *Cauchy stress* tensor which is related to strain through a material law as

$$\sigma = C(\varepsilon) \,. \tag{7}$$

In stable elastic equilibrium situations the total energy must be at a minimum [ZT00]. Mathematically, this can be reformulated by setting the first varitation of energy to zero, i.e. $\delta\Pi = 0$, which yields the virtual work equation

$$\int_\Omega \delta\varepsilon : C(\varepsilon) d\Omega - \int_\Omega \delta u \; f \; d\Omega + \int_\Omega \delta u \; \rho \; \ddot{u} \, d\Omega = 0 \,, \tag{8}$$

where the second term accounts for body forces per volume $f$ and the last term stands for inertial forces. This equation constitutes the basis for the subsequent finite element discretisation.

### 3.2. Thin Shell Mechanics

For the reader's convenience and in order to keep this work self contained we proceed with a quick overview of the Kirchhoff-Love shell theory. The following section is essentially a summary of Cirak et al. [COS00] and we will make deliberate use of notation and formulae used by them. For further details on the mechanics of thin shells the reader is generally referred to [WT03, SF89].

In the Kirchhoff-Love theory of thin shells the configuration mapping (1) is expressed in terms of the mid-surface parametrisation $\mathbf{x}(\theta^1,\theta^2)$ (see Figure 2) as

$$\varphi(\theta^1,\theta^2,\theta^3) = \mathbf{x}(\theta^1,\theta^2) + \theta^3\mathbf{a}_3(\theta^1,\theta^2)\,, \tag{9}$$

where $\theta^i$ denote curvilinear coordinates and $\mathbf{a}^3$ is the director field normal to the surface. In analogy to eq. (1) we write

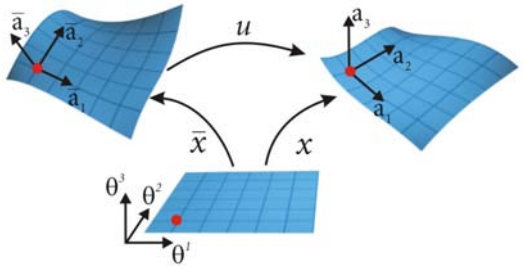


**Figure 2:** *A material point (red) on the shell's mid-surface with basis vector frame in the initial, reference, and current configuration (from left to right).*

$$\mathbf{x}(\theta^1,\theta^2) = \bar{\mathbf{x}}(\theta^1,\theta^2) + \mathbf{u}(\theta^1,\theta^2)\,. \tag{10}$$

From this, tangential surface basis vectors can be defined as

$$\mathbf{a}_\alpha = \mathbf{x}_{,\alpha}\,. \tag{11}$$

Moreover, the covariant tangent base vectors are given through differentiation of the configuration mapping as

$$\mathbf{g}_\alpha = \varphi_{,\alpha} = \mathbf{a}_\alpha + \theta^3\mathbf{a}_{3,\alpha} \tag{12}$$

from which the surface *metric tensor* is derived as

$$g_{ij} = \mathbf{g}_i \cdot \mathbf{g}_j. \tag{13}$$

Following eq. (4) this leads to the definition of the Green strain

$$\varepsilon^G_{ij} = \frac{1}{2}(g_{ij} - \bar{g}_{ij}) = \alpha_{ij} + \theta^3\beta_{ij}\,, \tag{14}$$

where $\alpha$ and $\beta$ are membrane and bending strains, respectively. In the Kirchhoff-Love theory, the director $\mathbf{a}_3$ is assumed to stay normal to the surface, straight and unstretched:

$$\mathbf{a}_3 = \frac{\mathbf{a}_1 \times \mathbf{a}_2}{|\mathbf{a}_1 \times \mathbf{a}_2|}\,. \tag{15}$$

Consequently, we have $\alpha_{3\beta} = \alpha_{\alpha 3} = 0$. The strains then simplify to

$$\alpha_{\alpha\beta} = \frac{1}{2}(\mathbf{a}_\alpha \cdot \mathbf{a}_\beta - \bar{\mathbf{a}}_\alpha \cdot \bar{\mathbf{a}}_\beta), \quad \beta_{\alpha\beta} = (\bar{\mathbf{a}}_{\alpha,\beta} \cdot \bar{\mathbf{a}}_3 - \mathbf{a}_{\alpha,\beta} \cdot \mathbf{a}_3)\,.$$

Departing from $\mathbf{a}_\alpha = \bar{\mathbf{x}}_{,\alpha} + \mathbf{u}_{,\alpha}$ and neglecting nonlinear terms, this can be recast to an expression which is linear in displacements [COS00, eq.(21) and (22)]. Resultant membrane and bending stresses follow as

$$n^{\alpha\beta} = \frac{\partial\Psi}{\partial\alpha_{\alpha\beta}}\,, \quad m^{\alpha\beta} = \frac{\partial\Psi}{\partial\beta_{\alpha\beta}}\,, \tag{16}$$

where $\Psi$ is the strain energy density. The particular form of $\Psi$ depends on the material law used. In this work we used a linear isotropic stress-strain relationship which leads to

$$\sigma = \mathcal{C}\varepsilon\,, \tag{17}$$

where $\mathcal{C}$ can be written in terms of the Lamé coefficients $\lambda$ and $\mu$ as $\mathcal{C}_{ijkl} = \lambda\delta_{ij}\delta_{kl} + 2\mu\delta_{ik}\delta_{jl}$.

### 3.3. Strain measures

Introducing the deformation gradient $F$ as

$$F = \frac{\partial\varphi}{\partial\bar{\varphi}}$$

eq. (4) can be alternatively written in the form

$$\varepsilon^G = \frac{1}{2}(F^TF - id) \tag{18}$$

(see [BW97]). Via polar decomposition $F$ can be split into a rotational part $R$ and a pure deformation $U$ as $F = RU$. From this, it can be seen that $\varepsilon^G$ is invariant under rotations since

$$F^TF = U^TR^TRU = U^TU \tag{19}$$

due to the orthogonality of $R$. The linearisation of the Green strain tensor $\varepsilon^G$ yields the *Cauchy* strain tensor

$$\varepsilon^C = \frac{1}{2}(\nabla u^T + \nabla u). \tag{20}$$

This tensor is linear in displacements but not rotationally invariant anymore. However, if the rotation field $R$ is known, the corotational strain formulation can be used and we obtain the rotated linear strain tensor:

$$\varepsilon^{CR}(\varphi) = \varepsilon^{CR}(R^T\varphi). \tag{21}$$

Determining this rotation field is crucial for our calculation and will therefore be detailed in section 4.3.

## 4. Subdivision-Based Finite Elements

This section explains how to construct the subdivision-based finite element solution of the virtual work equation (8). Although well known to computer graphics, the concept of subdivision is briefly recapitulated, as well as the actual spatial discretisation. The extraction of rotations from the displacement field is detailed subsequently and finally, the incorporation of boundary conditions is discussed.

### 4.1. Subdivision Surfaces

Subdivision is a process for constructing smooth limit surfaces through successive refinement of an initial control mesh. This procedure essentially consists of two steps: first, the geometry is refined through introduction of new nodes and second, new nodal positions are computed. For a discussion of the diversity of subdivision schemes we refer the reader to [ZS00]. Here, we limit our attention to Loop's subdivision scheme because it was used in the approach by Cirak et al [COS00] which is the basis for this work.

Loop's scheme is approximating, i.e. the nodes of the mesh at a coarser level are not contained in meshes at finer levels. However, besides the usual $C^1$-continuity inherent to subdivision surfaces the curvature is $L_2$- or square integrable [RS01]. Due to this property, the subdivision basis functions can be used as shape functions for the FE-solution of the thin shell equations. In each step of this subdivision method, the positions of newly inserted nodes as well as those of old nodes are computed through a linear combination of vertices from the coarse mesh determined by the so called subdivision mask. In the case of Loop subdivision

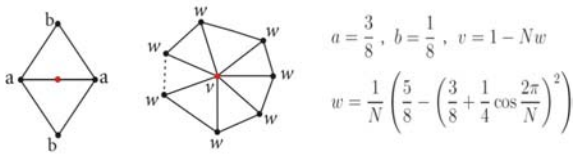


**Figure 3:** *Subdivision masks.* Left*: Edge mask to determine new vertex.* Middle*: Mask for vertex with valence N.*

only the immediate neighbours (i.e. the 1-ring) of a vertex have influence on this computation which gives rise to an efficient implementation. The corresponding vertex masks for computing the new positions are shown in Figure 3. The subdivision process can be considered as a linear operator and consequently be written in matrix form. It is therefore possible to directly derive properties like derivatives of the limit surface using an Eigenanalysis of the subdivision matrix. This yields simple expressions that can be computed efficiently (see Figure 4). Besides the evaluation at the nodes

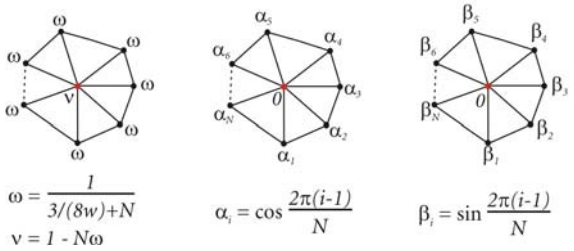


**Figure 4:** Left*: Limit mask for a vertex of valence N.* Middle *and* right*: Masks for associated tangent vectors.*

these quantities can also be determined at the interior of the triangles. The key observation is that in regular settings (i.e. when all involved vertices have valence 6) Loop's scheme leads to generalised quartic box splines. In this case surface properties in one triangle (or *patch*) are completely defined through the 12 nodal values in the 1-neighbourhood (see Figure 5) and the associated box spline basis functions $N_i$.
For instance, if we denote the local patch coordinates by $\theta^\alpha$, the limit surface can be expressed as

$$\mathbf{x}(\theta^1,\theta^2) = \sum_i^{12} N_i(\theta^1,\theta^2)\mathbf{x}_i \,, \tag{22}$$

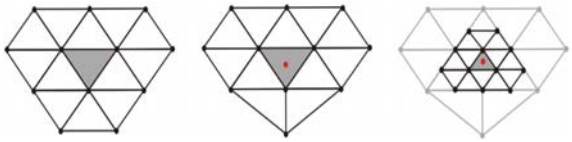

**Figure 5:** Left*:1-neighbourhood of a regular patch consisting of 12 nodes.* Middle*: Irregular patch with one vertex of valence 5.* Right*: After a single local sudivision step the barycenter (depicted in red) lies again in a regular neighbourhood.*

where $\mathbf{x}_i$ are the nodal positions of the underlying mesh. In the same way, the displacement field interpolation is obtained from the nodal values. Additionally, differential quantities can be determined as

$$\mathbf{x}_{,\alpha}(\theta^1,\theta^2) = \sum_i^{12} N_{i,\alpha}(\theta^1,\theta^2)\mathbf{x}_i \,. \tag{23}$$

If the patch has an irregular vertex the box spline assumption no longer holds and thus interior parameter points cannot be evaluated. For the following finite element discretisation, however, only quantities at the barycenter of the triangles are needed for integral evaluation. Hence, Cirak et al. required the initial mesh to have at most one irregular vertex per triangle. Then, after one subdivision step the barycenter lies again inside a regular patch (see Figure 5). This process of subdivision and evaluation of the newly generated patch can again be expressed as a sequence of matrix multiplications. Though sufficient for this case, the method can be extended to quantity evaluation at arbitrary parameter values using the technique proposed by Stam [Sta98].

### 4.2. Spatial Discretisation

For the sake of completeness we recapitulate the spatial discretisation of the underlying PDE which was derived in [COS00].

With the definition of the membrane and bending strains and assuming a linear elastic material (eq. (17)) the internal energy from eq. (8) can be rewritten as

$$\int_\Omega \delta\varepsilon : C(\varepsilon) d\Omega = \int_\Omega \left(\delta\alpha^T \mathbf{H}_m \alpha + \delta\beta^T \mathbf{H}_b \beta\right) d\Omega \,, \tag{24}$$

where $\mathbf{H}_m$ and $\mathbf{H}_b$ are matrices corresponding to the membrane and bending part of the material law. Due to the linear strain interpolation, we have

$$\alpha(\theta^1,\theta^2) = \sum_i^N \mathbf{M}_i(\theta^1,\theta^2)\mathbf{u}_i, \quad \beta(\theta^1,\theta^2) = \sum_i^N \mathbf{B}_i(\theta^1,\theta^2)\mathbf{u}_i$$

for matrices $\mathbf{M}_i$ and $\mathbf{B}_i$ relating nodal displacements $\mathbf{u}_i$ to membrane and bending strain. This gives rise to a formulation of the complete system in the classical form of

$$\mathbf{K}\mathbf{u} = \mathbf{f} \tag{25}$$

with vectors of nodal displacement $\mathbf{u}$ and forces $\mathbf{f}$. The stiffness matrix $\mathbf{K}$ can be assembled in the usual element-wise

fashion

$$\mathbf{K}_{ij} = \sum_e \int_{\Omega_e} \left( \mathbf{M}_i^T \mathbf{H}_m \mathbf{M}_j + \mathbf{B}_i^T \mathbf{H}_b \mathbf{B}_j \right) d\Omega = \sum_e \mathbf{K}_{ij}^e \,. \quad (26)$$

The integral in this equation can be evaluated using numerical quadrature. We point out that due to the compact support of the shape functions, only a finite number of elements have a non-zero contribution to $\mathbf{K}_{ij}$. This leads to a sparse matrix system for which efficient solvers are available. Although more accurate schemes are possible, we follow Cirak et al. and use a one-point quadrature rule at the center of the triangles. In this form, the above equations are only valid on regular patches. However, as mentioned above, in irregular settings one subdivision step is sufficient for evaluations at the barycenters. For a patch with irregular vertex of valence $N$ let $\mathbf{S}$ denote the the subdivision operator (see [COS00]). Further, let $\mathbf{P}$ be the projection operator extracting the 12 vertices corresponding to the central regular subpatch (Figure 5, right). Then we can write

$$\mathbf{K}_{ij}^e = \int_{\Omega_e} \left[ \mathbf{S}^T \mathbf{P}^T \left( \mathbf{M}_i^T \mathbf{H}_m \mathbf{M}_j + \mathbf{B}_i^T \mathbf{H}_b \mathbf{B}_j \right) \mathbf{P} \mathbf{S} \right] d\Omega \quad (27)$$

and thus simply include the conceptual subdivision step into the stiffness matrix.

To cover dynamic effects of moving and deforming objects inertial as well as viscous forces have to be included. This leads to the second order ordinary differential equation (ODE) in time

$$\Lambda \ddot{\mathbf{u}}_n + \mathbf{D}\dot{\mathbf{u}}_n + \mathbf{K}\mathbf{u} = \mathbf{f} \,, \quad (28)$$

where $\Lambda$ is the diagonal nodal mass matrix obtained via mass lumping and $\mathbf{D}$ is the viscosity matrix. We use a viscous tensor proportional to the elasticity tensor, $\mathcal{D} = \nu\mathcal{C}$, which is derived from the Kelvin-Voigt material model [HGSB03]. For the numerical solution, eq. (28) is transformed into a set of coupled first order ODEs and the implicit Euler time integration scheme is applied. The arising system of linear equations (LES) with nodal velocities as primary unknowns is solved using the conjugate gradient method (details to the theory and implementation can be found in [EKS03]).

### 4.3. Corotational Formulation

Provided the deformations stay small throughout the simulation they can be approximated using a linear displacement formulation. While this is a reasonable assumption for the in-plane deformation (i.e. stretching and shearing) of cloth, any practical application will most likely lead to large bending deformations and rigid body transformations, including rotation. Since the Cauchy strain is not rotationally invariant, one has to extract the rotations from the displacement field as mentioned above in eq. (21).

With the definition of the configuration mapping (eq. (9)) the deformation gradient can be written as

$$F = \frac{\partial \varphi}{\partial \bar{\varphi}} = \frac{\partial \varphi}{\partial \theta^i} \otimes \bar{\mathbf{g}}^i = \left[ \mathbf{a}_\alpha + \theta^3 \mathbf{a}_{3,\alpha} \right] \otimes \bar{\mathbf{g}}^\alpha + \mathbf{a}_3 \otimes \bar{\mathbf{g}}^3 \,, \quad (29)$$

where $\bar{\mathbf{g}}^i$ are the contravariant basis vectors which are related to their covariant counterparts via $\bar{\mathbf{g}}^i \cdot \bar{\mathbf{g}}_j = \delta_{ij}$ (see [WT03]). In this form, the deformation gradient is a $(3 \times 3)$-tensor and its polar decomposition would necessitate the use of an iterative scheme [HS04]. In our case, we want to further exploit the inherent two-dimensionality of the problem. The assumed kinematic restrictions on the shell (i.e. that the director remains straight, normal and unstretched) effectively render the decomposition problem two-dimensional since we have for the resulting stretch tensor

$$\mathbf{U} = \begin{bmatrix} U_{11} & U_{12} & 0 \\ U_{12} & U_{22} & 0 \\ 0 & 0 & 1 \end{bmatrix} \,. \quad (30)$$

From eq. (19) we can thus deduce that only the $(2 \times 3)$-submatrix $\tilde{\mathbf{F}}$ will be relevant for the computation of $\mathbf{U}^2$. We therefore compute the principal stretches in the 2D subspace and find the rotation $\tilde{\mathbf{R}}$ which transforms the element from the initial (flat) configuration to its current position by

$$\tilde{\mathbf{R}} = \tilde{\mathbf{F}} \tilde{\mathbf{U}}^{-1} \,, \quad (31)$$

where $\tilde{\mathbf{U}}$ is the upper $(2 \times 2)$ submatrix of $\mathbf{U}$.

In the presented approach, the deformation gradient is not constant over an element and thus, theoretically, rotations might be different for each vertex. However, we found that using the rotation obtained for the barycenter of the patch for all the vertices involved was sufficient in all of our tests. Only in the case of very inhomogeneous deformation this might lead to noticeable approximation errors which, again, did not appear in practice.

### 4.4. Boundary Conditions

The evaluation of integrals (appearing in eq. (26)) for elements on the border of the domain requires special versions of the subdivision rules. To avoid the treatment of these special cases Cirak et al. suggest the use of a method proposed by Schweitzer [Sch96] which introduces a layer of artificial vertices around the boundary. The positions of these vertices are calculated from their original neighbours such that the application of the normal subdivision rules effectively reproduces the behaviour of the border rules. When imposing boundary conditions, i.e. constraints on the boundary nodes, the artificial vertices have to be taken into account. The case of a fixed boundary with rotations allowed (simply supported) is depicted in Figure 6 (for an in depth discussion of boundary conditions see [GT04]). Now, if the equation system arising from (28) is to be solved using an iterative scheme like the conjugate gradient method, this interdependence between the input variables actually hinders the convergence and might even lead to divergence. Fortunately, this inconvenience can be circumvented through elimination of the boundary vertices from the equation system and subsequent symmetrization through elemental matrix transformations.

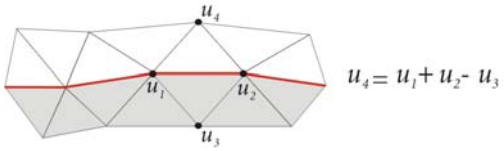


**Figure 6:** *Connectivity of an artificial vertex $u_4$ around the boundary (shown in red). The displacement of $u_4$ is determined by its local neighbours. In the example, the border is fixed while allowing rotations.*

## 5. Computational Classification

In this section we give a brief account of the computational complexity of our method in comparison with standard linear finite element approaches. It is worth noting that the build-up process for the matrix **K** in eq. (27) is very similar to a common FE-formulation. Since the elemental submatrices are assembled into the global stiffness matrix in an additive way, the same framework can be used. The evaluation cost for an element matrix in our approach is slightly higher than for usual methods. This is mainly due to the increased connectivity of the elements: a regular patch contains a neighbourhood of 12 nodes where for standard approaches there are only three. This means, that more entries have to be computed and written into the system matrix. In the course of numerous test cases we found out that, as a partial remedy, the condition of the resulting LES is improved. Hence, fewer iterations are necessary to solve the system. Additionally, even with coarser meshes our method delivers superior results compared to standard FE-approaches, especially in buckling situations (cf. Fig. 1). This also makes up for a part of the costs spent in the assembly stage. As an example, we provide the actual computation times for the compression scene (see Fig. 11) where we used a mesh with 2542 vertices and a step size of $0.01s$. We used an AMD Athlon64 (2200 MHz) based system with 1GB of main memory. One simulation second took about $245s$ with our method and about $79s$ with the FE-approach by Etzmuss et al. While this is roughly a factor of three for the physical simulation, we point out that processing times for collision detection and response can be much larger. This is especially the case when complicated self collisions occur (see the accompanying video). In this case the additional costs of our method are less significant. Lastly, we recall that this approach is not aimed at real-time animations but at physically accurate simulation. The advantages over previous approaches offered by our method have to be weighted against the increased complexity. We believe that if accuracy is more important than speed the benefits by far outweigh the drawbacks.

## 6. Results

In this section we present the results obtained from our corotational subdivision-based FE-method for cloth simulation. Unless stated otherwise, we used a standard cotton material with elasticity coefficient (Young's modulus) $E = 5000N/m$ and Poisson's ratio $\nu = 0.25$ obtained from Kawabata measurements [Kaw80] of real fabric samples. For the time integration we used the implicit Euler method with a step size of $0.001s$. Even for large deformations (see e.g. 11) stability was never a problem. In fact, for the test scenes without collisions even a step size of $0.01s$ led to good results. For scenes where collisions occur we use a bounding volume hierarchy detection scheme based on k-dops [MKE03]. The collision response is an implementation of the robust method by Bridson et al. [BFA02]. This approach incorporates a subdivision postprocess for smoothing sharp folds which fits nicely into our simulation framework. Below, we mainly show snapshots taken from the dynamic scenes we produced. A more comprehensive set of examples can be found in the accompanying video.

In our dynamic test scenarios we chose cylindrical sleeves, which are frequently encountered with clothes, as basic primitives (see Figures 1,7,9,10,11). This gives us a well defined case to investigate the quality of our approach with respect to static buckling and folding situations and compare them to real test scenarios (Figure 1). We believe that the capability of modelling these kinds of features is crucial for any cloth simulation technique. In the second part of this section we validate our method through the application to standard clothes like a sweater or a pair of trousers (see Figure 12).

**Figure 7:** *Different types of folds on a garment's sleeve generated by our method.* Left*: Catenary-shaped folds due to gravitational forces.* Middle*: Diagonal folds resulting from torsional deformation at one end.* Right: *Buckling due to compressive deformation.*

In the first set of examples (Figure 7), a fabric sleeve is subjected to gravitational loading and shows the expected catenary-shaped folds (left). The sleeve is then wrung, showing distinct diagonal folds (middle) and finally compressed, neglecting forces due to gravitation (right). The specific folds expected in this situation are clearly reproduced by our method and very similar behaviour can be observed with real fabrics. The geometric model used in these examples consists of only 494 vertices and is, compared to the detail of the results, relatively coarse for standard cloth simulation. Experiments with finer discretisations did not substantially affect the visual quality of the results. This is due to the fact that using higher order elements, globally nonlinear effects can already be captured on a coarser scale compared to simpler linear elements (cf. [MS06]). The global shape of the results obtained from our simulation is undoubtably due to the consistent way of modelling bending energy. This can also

be seen in Figure 1 which shows a test case where buckling occurs due to compressive deformation. Here, the salient features are the diamond-shaped buckling patterns. In reality (lefmost picture), the size and the number of patterns that occur depend on the material properties, the thickness and the radius. With our method (second from left) these effects can be captured realistically. The second illustration from the right was computed with a standard FE-approach with linear basis functions using the bending model of [EKS03]. Clearly, the expected folds cannot be reproduced satisfactorily with the simple model. Moreover, using a finer mesh does not help as can be seen in the rightmost example of Figure 1. The global shape which in this case is dominated by the size and the number of diamond-shaped folding patterns changes significantly for different resolutions. This is not the case for our method. The relative discretisation independence of our method can also be seen in Figure 8.

**Figure 8:** *Front view of twisted fabric sleeves made of different materials.* Left: *a thin,* middle: *a ten times thicker material.* Right*: as in the middle but with a ten times stronger stretch resistance. The number of folds varies with the material parameters although the same mesh was used.*

Here, it is interesting to note that the number of folds appearing in consequence to torsional deformation only depends on material parameters and not on the discretisation. In all three cases we used the same mesh consisting of 1500 triangles and we applied the same amount of torsion. The number of folds however varies with different material parameters and thickness. In fact, this behaviour is not accidental but derives from the buckling properties of cylindrical shells [AP04]. During the course of further experiments with different materials we noticed that quite a broad range can be reproduced convincingly (see Figure 10 and 11).

We also carried out further experiments highlighting the different deformation modes and features of our method. Figure 9 shows some snapshots from an animation in which a sleeve is subjected to torsional deformation. One can clearly notice the forming of folds starting with fine wrinkles which merge into bigger folds.

**Figure 9:** *Sequence with increasing torsional deformation of a sleeve.*

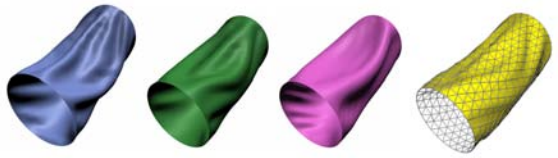

**Figure 10:** *Fabric sleeves under gravitational loading with different material parameters.* Right*: Mesh used in computation with 494 Vertices and 936 faces.*

**Figure 11:** *Sequence taken from an animation of axial compression of a sleeve with a metal-like material.*

Additionally, we ran a simulation of the sleeve compression scene with the parameter set of $E = 100000N/m, \nu = 0.05$ and a thickness of $1mm$, leading to a behaviour similar to thin flexible metal (see Figure 11). Hence, it is possible to visually differentiate between different material types by merely considering the drape and deformation of the object.

In the second part we verified our approach with common garments such as a sweater or a pair of trousers. The

**Figure 12:** Left*: woman wearing a sweater.* Right*: a pair of trousers pinned at the legs is hanging vertically.*

trousers and the sweater consist of 1000 and 1600 vertices respectively. The pair of trousers is fixed at the ends of the extremities and is subjected to gravity (see Figure 12). Here, naturally appearing folds and wrinkles are obtained and catenary folds as well as buckling patterns can be observed. Despite the rather coarse discretisation of the mesh used in this example detailed features and, at the same time, convincing global appearance can be reproduced without any need for

post-processing or non-physical intervention. The left hand side of the figure shows one frame of a virtual try-on sequence of a pullover on a person where the interaction of our simulation with the collision handling can be observed.

## 7. Conclusion and Future Work

We proposed a method for consistently modelling membrane and bending energies arising in the simulation of thin, flexible objects such as cloth. With the advent of subdivision-based finite elements, cloth simulation can now be founded on the physically sound basis of the thin shell equations which covers stretching, shearing, and bending in one consistent theory. A novel achievement of the presented work is the combination of this new paradigm with a corotational strain formulation resulting in a completely linear system which, in turn, leads to an efficient implementation. Since the time integration of all forces (resp. energies) is carried out implicitly unconditional stability can be guaranteed. The presented examples clearly demonstrate the advantages of the presented method above previous approaches: when phenomena highly dependent on bending properties are encountered, e.g. the buckling of fabric, usual methods fail without further non-physical intervention while our approach shows the expected behaviour. Furthermore, common post-processing steps can be integrated in a very elegant way, if desired. Since the employed subdivision basis leads to smooth limit surfaces, the geometry can be locally evaluated and refined to the desired degree.

A limitation of the presented method is that the limit surface does not interpolate the vertices of the control mesh. This may become inconvenient if e.g. a garment is assembled from flat patterns in a CAD application and the resulting mesh is used as the control mesh. This shortcoming could be resolved in a preprocessing step in which the control mesh is transformed such that the limit surface approximates best the originally designed garment mesh. A further restriction is that we are currently using the control mesh for collision detection. This, of course, is not as accurate as using the limit surface itself. However, if the control mesh is not too coarse this effect can safely be neglected and we have not encountered any problems in our test cases. Although we obtained good results even in the presence of complicated self collisions, the use of a specifically designed collision detection scheme is an option for future work (cf. [GS01]).

The implementation effort and computational costs for our method are higher than for mass-spring or particle systems. However, we believe that our method has strong arguments when it comes to trading accuracy for computational speed: while current computation times are certainly beyond the interactive range the physical fidelity and versatility offered by this method can be of great interest to anyone wishing to reproduce fabric behaviour in an accurate way. A closer investigation and quantitative evaluation of our solution for different material types would be interesting as well. One part of our ongoing research is the comparison of real to virtual material parameters. Here, the goal is to re-obtain the same material parameters in virtual measurements as in the corresponding real measurements, which where originally used as input for the model. Additionally, the application of multi-resolution numerics is a very promising extension (cf. [GTS02]) which motivates expectations on highly increased computational efficiency.

## 8. Acknowledgements

This work was partially supported by grants of the Landesstiftung Baden-Württemberg which are gratefully acknowledged by B. Thomaszewski and M. Wacker. Additionally, the first author was supported by a grant of the Thomas-Gessmann-Stiftung. The authors would like to thank Francois Faure for valuable discussions and support.

## References

[AP04] K. Athiannan and R. Palaninathan. Experimental investigations on buckling of cylindrical shells under axial compression and transverse shear. *Sadhana*, pages 93–115, February 2004.

[Bar89] A. H. Barr. The einstein summation notation: Introduction and extensions. In *SIGGRAPH '89 Course Notes on Topics in Physically-Based Modeling*, volume 30, pages J1–J12, 1989.

[BFA02] R. Bridson, R. Fedkiw, and J. Anderson. Robust treatment of collisions, contact and friction for cloth animation. In *Proceedings of ACM SIGGRAPH '02*, pages 594–603. ACM Press, 2002.

[BHW94] D. Breen, D. House, and M. Wozny. Predicting the drape of woven cloth using interacting particles. In *Proceedings of ACM SIGGRAPH '94*, pages 365–372. ACM Press, 1994.

[BMF03] R. Bridson, S. Marino, and R. Fedkiw. Simulation of clothing with folds and wrinkles. In *Proceedings of ACM SIGGRAPH/Eurographics Symposium on Computer Animation (SCA 2003)*, pages 28–36. ACM Press, 2003.

[BW97] J. Bonet and R. D. Wood. *Nonlinear Continuum Mechanics for Finite Element Analysis*. Cambridge University Press, 1997.

[BW98] D. Baraff and A. Witkin. Large steps in cloth simulation. In *Proceedings of ACM SIGGRAPH '98*, pages 43–54. ACM Press, 1998.

[CK02] Kwang-Jin Choi and Hyeong-Seok Ko. Stable but responsive cloth. In *Proceedings of ACM SIGGRAPH '02*, pages 604–611. ACM Press, 2002.

[CO01] F. Cirak and M. Ortiz. Fully $C^1$-conforming subdivision elements for finite deformation thin-shell analysis. *Journal for Numerical Methods in Engineering*, 51:813–833, 2001.

[COS00] F. Cirak, M. Ortiz, and P. Schröder. Subdivision surfaces: A new paradigm for thin-shell finite-element analysis. *Journal for Numerical Methods in Engineering*, 47:2039–2072, 2000.

[EDC96] J. Eischen, S. Deng, and T. Clapp. Finite-element modeling and control of flexible fabric parts. *IEEE Computer Graphics and Applications*, 16(5):71–80, September 1996.

[EKS03] O. Etzmuss, M. Keckeisen, and W. Straßer. A Fast Finite Element Solution for Cloth Modelling. In *Proceedings of Pacific Graphics*, pages 244–251, 2003.

[GCSO99] E. Grinspun, F. Cirak, P. Schröder, and M. Ortiz. Non-linear mechanics and collisions for subdivision surfaces. Technical report, Caltech Multi-Res Modeling Group, 1999.

[GH+03] E. Grinspun, , A. Hirani, M. Desbrun, and P. Schröder. Discrete shells. In *Proceedings of ACM SIGGRAPH/Eurographics Symposium on Computer Animation (SCA 2003)*, pages 62–67. ACM Press, 2003.

[GS01] E. Grinspun and P. Schröder. Normal bounds for subdivision-surface interference detection. In *Proceedings of IEEE Visualization '01*, pages 333–340. IEEE Computer Society, 2001.

[GT04] S. Green and G. Turkiyyah. Second-order accurate constraint formulation for subdivision finite element simulation of thin shells. *International Journal for Numerical Methods in Engineering*, 61(3):380–405, 9 2004.

[GTS02] S. Green, G. Turkiyyah, and D. Storti. Subdivision-based multilevel methods for large scale engineering simulation of thin shells. In *SMA '02: Proceedings of the seventh ACM symposium on Solid modeling and applications*, pages 265–272. ACM Press, 2002.

[HB00] D. H. House and D. E. Breen, editors. *Cloth modeling and animation*. A. K. Peters, Ltd., Natick, MA, USA, 2000.

[HGSB03] Michael Hauth, Joachim Groß, Wolfgang Straßer, and Gerhard F. Buess. Soft tissue simulation based on measured data. In *Proceedings of MICCAI (1)*, pages 262–270, 2003.

[HS04] M. Hauth and W. Straßer. Corotational simulation of deformable solids. *Journal of WSCG*, 12(1):137–145, 2004.

[Kaw80] S. Kawabata. *The Standardization and Analysis of Hand Evaluation*. The Textile Machinery Society of Japan, Osaka, 1980.

[MDM+02] M. Müller, J. Dorsey, L. McMillan, R. Jagnow, and B. Cutler. Stable real-time deformations. In *Proceedings of the 2002 ACM SIGGRAPH/Eurographics symposium on Computer animation (SCA 2002)*, pages 49–54. ACM Press, 2002.

[MKE03] Johannes Mezger, Stefan Kimmerle, and Olaf Etzmuß. Hierarchical Techniques in Collision Detection for Cloth Animation. *Journal of WSCG*, 11(2):322–329, 2003.

[MS06] Johannes Mezger and Wolfgang Straßer. Interactive Soft Object Simulation with Quadratic Finite Elements. In *IV Conference on Articulated Motion and Deformable Objects (AMDO)*, 2006. Accepted for publication.

[NG96] H. N. Ng and R. L. Grimsdale. Computer graphics techniques for modeling cloth. *IEEE Comput. Graph. Appl.*, 16(5):28–41, 1996.

[RS01] U. Reif and P. Schröder. Curvature integrability of subdivision surfaces. *Advances in Computational Mathematics*, 14(2):157–174, 2001.

[Sch96] J. E. Schweitzer. *Analysis and application of subdivision surfaces*. PhD thesis, Department of Computer Science and Engineering, University of Washington, Seattle, 1996.

[SF89] J. C. Simo and D. D. Fox. On stress resultant geometrically exact shell model. part i: formulation and optimal parametrization. *Comput. Methods Appl. Mech. Eng.*, 72(3):267–304, 1989.

[Sta98] J. Stam. Evaluation of loop subdivision surfaces. In *SIGGRAPH '98 CDROM Proceedings*, 1998.

[VCMT95] P. Volino, M. Courchesne, and N. Magnenat-Thalmann. Versatile and efficient techniques for simulating cloth and other deformable objects. In *Proceedings of ACM SIGGRAPH '95*, pages 137–144. ACM Press, 1995.

[VCMT05] P. Volino, F. Cordier, and N. Magnenat-Thalmann. From early virtual garment simulation to interactive fashion design. *Computer-Aided Design Journal, Elsevier*, 37:593–608, 2005.

[VMT00] Pascal Volino and Nadja Magnenat-Thalmann. *Virtual Clothing*. Springer, 2000.

[WSG05] M. Wicke, D. Steinemann, and M. Gross. Efficient animation of point-sampled thin shells. *Computer Graphics Forum (Eurographics 2005)*, 24(3):667–676, September 2005.

[WT03] G. Wempner and D. Talaslidis. *Mechanics of solids and shells: Theories and approximations*. CRC Press, 2003.

[ZS00] D. Zorin and P. Schröder. Subdivision for Modeling and Animation. In *SIGGRAPH '00 Course Notes*, 2000.

[ZT00] O.C. Zienkiewicz and R.L. Taylor. *The Finite Element Method. Volume 1: The Basis*. Butterworth Heinemann, 5th edition, 2000.